



UNIVERSITY OF LEEDS

This is a repository copy of *Control of steam input to the pyrolysis-gasification of waste plastics for improved production of hydrogen or carbon nanotubes*.

White Rose Research Online URL for this paper:
<http://eprints.whiterose.ac.uk/80719/>

Article:

Acomb, JC, Wu, C and Williams, PT (2014) Control of steam input to the pyrolysis-gasification of waste plastics for improved production of hydrogen or carbon nanotubes. *Applied Catalysis B: Environmental*, 147. 571 - 584. ISSN 0926-3373

<https://doi.org/10.1016/j.apcatb.2013.09.018>

Reuse

Unless indicated otherwise, fulltext items are protected by copyright with all rights reserved. The copyright exception in section 29 of the Copyright, Designs and Patents Act 1988 allows the making of a single copy solely for the purpose of non-commercial research or private study within the limits of fair dealing. The publisher or other rights-holder may allow further reproduction and re-use of this version - refer to the White Rose Research Online record for this item. Where records identify the publisher as the copyright holder, users can verify any specific terms of use on the publisher's website.

Takedown

If you consider content in White Rose Research Online to be in breach of UK law, please notify us by emailing eprints@whiterose.ac.uk including the URL of the record and the reason for the withdrawal request.



eprints@whiterose.ac.uk
<https://eprints.whiterose.ac.uk/>

Control of steam input to the pyrolysis-gasification of waste plastics for improved production of hydrogen or carbon nanotubes

Jonathan C. Acomb, Chunfei Wu and Paul T. Williams*

Energy Research Institute,
University of Leeds, Leeds LS2 9JT, UK.

*(Email: p.t.williams@leeds.ac.uk; Tel: #441133432504; FAX: #44132467310)

ABSTRACT

Carbon nanotubes (CNTs) have been proven to be possible as high-value by-products of hydrogen production from gasification of waste plastics. In this work, steam content in the gasification process was investigated to increase the quality of CNTs in terms of purity. Three different plastics - low density polyethylene (LDPE), polypropylene (PP) and polystyrene (PS) were studied in a two stage pyrolysis-gasification reactor. Plastics samples were pyrolysed in nitrogen at 600°C, before the evolved gases were passed to a second stage where steam was injected and the gases were reformed at 800°C in the presence of a nickel-alumina catalyst. To investigate the effect that steam plays on CNT production, steam injection rates of 0, 0.25, 1.90 and 4.74 g h⁻¹ were employed. The CNTs produced from all three plastics were multiwalled CNTs with diameters between 10 and 20 nm and several microns in length. For all the plastic samples, raising the steam injection rate led to increased hydrogen production as steam reforming and gasification of deposited carbon increased. High quality CNTs, as observed from TEM, TPO and Raman spectroscopy, were produced by controlling the steam injection rate. The largest yield for LDPE was obtained at 0 g h⁻¹ steam injection rate, whilst PP and PS gave their largest yields at 0.25 g h⁻¹. Overall the largest CNT yield was obtained for PS at 0.25 g h⁻¹, with a conversion rate of plastic to CNTs of 32% wt.

1 Introduction

Management of plastic waste poses a serious challenge for society as plastics make up a significant proportion of municipal waste, typically around 10 wt% [1]. Even though recycling rates for waste plastics have recently increased [2] there is still a large amount which ends up being unsustainably disposed of in landfill sites. With governments imposing stricter limitations on landfilling, other waste management techniques are required.

A desirable alternative to landfilling of plastic waste is chemical recycling of plastics through thermal treatments such as pyrolysis and gasification. These processes can be used to produce valuable materials such as gases and oils for use in energy applications [3-5]. Hydrogen gas is of particular interest as it is seen as an important future fuel since its combustion gives off no CO₂. The production of hydrogen from thermal treatment of plastics has been researched, with polyethylene, polypropylene and polystyrene among the feedstocks investigated [6-14]. High hydrogen yields can be obtained, for example it has been reported that the hydrogen content of gases produced from various plastics was above 60 Vol.% when a Ni-Mg-Al catalyst was used in a two stage pyrolysis-gasification procedure [14]. Czernik and French likewise made use of a nickel catalyst and obtained 80% of the theoretical maximum hydrogen production from a polypropylene source [7]. The effect of increasing the steam/plastic ratio was investigated by Erkiaga et al using a high density polyethylene in a conical spouted bed reactor [8]. It was seen that as the steam/plastic ratio was increased the amount of tars and char reduced whilst seeing an increase in the amount of gases and hydrogen produced. Nickel catalysts are particularly good catalysts for hydrogen production from steam reforming as they give much higher yields than other transition metals such as copper and iron, but are cheaper than other effective catalysts such as ruthenium [15].

Carbon deposition on the surface of nickel catalysts poses a major challenge to hydrogen production, since it can deactivate the catalyst. Rostrup-Nielsen [16] identified three types of

carbon deposition, whisker type carbons, such as filamentous carbons, in addition to pyrolytic and encapsulating carbons which deactivate the catalyst. Our previous studies on the production of H₂ from plastics have shown the carbon deposits produced are predominantly filamentous carbons [12, 17]. We have recently confirmed, using transmission electron microscopy (TEM) analysis of the filaments, the presence of carbon nanotubes (CNTs) on the surface of the catalyst, and a process was developed to produce CNTs and hydrogen simultaneously [18]. The simultaneous production of CNTs and hydrogen from plastic feedstocks increases the efficiency and economic value of the process.

Carbon nanotubes are a material that have been studied a great deal since their discovery by Sumio Iijima in 1991 [19] due to their potential for future uses in a number of mechanical, thermal and electronic applications [20]. CNTs are thought to be formed by a modified version of the vapour-liquid-solid mechanism proposed by Baker et al [21, 22]. A vapour-solid-solid mechanism has been proposed where carbon dissociates on the surface of a catalyst particle, diffuses across its surface and finally precipitates in the form of CNTs [23].

The injection of steam is a crucial factor in production of both hydrogen and CNTs. Previous work has shown that increasing the steam injection rate leads to an increase in the production of hydrogen from plastic waste via steam reforming [24]. Likewise the addition of steam is key in the production of CNTs [25, 26]. Hata et al [26] found that steam acts as a weak oxidiser, reacting with amorphous carbons which deactivate the catalyst, enabling longer and purer CNTs to grow. Ago et al [25] varied steam injection and found that increasing the amount of steam increases the yield of CNTs up to a critical concentration at which point the yield drastically fell. It was suggested that at this point the water deactivated the catalyst and restricted the deposition of methane. As such, whilst the injection of steam can be beneficial to the production of CNTs, the amount of steam injected is a crucial factor in obtaining a large yield.

CNT production from plastics has been demonstrated [27-38], however the effect of the steam injection rate on CNT and hydrogen has not been considered. The potential to produce CNTs from the pyrolysis of plastics was demonstrated by Kukovitsky et al [27]. Generating CNTs from waste plastics holds the benefit of simultaneously dealing with waste management problems, and also providing a cheap and abundant feedstock for CNT production. Kukovitsky et al used granular polyethylene (PE) which was pyrolysed with a nickel catalyst at temperatures of 420-450°C. Whilst CNTs were produced, the yield was small with the majority of the deposits being carbon fibres. Later work by the same research group obtained a larger CNT yield at the higher temperature of 800°C [32].

Subsequently further studies have been undertaken to produce CNTs from plastic sources. Chung et al [35] investigated the use of both polypropylene (PP) and polystyrene (PS) as CNT precursors. CNTs were produced from each of the plastics, however the morphology of the CNTs varied depending on the feedstock due to the aromatic and olefinic nature of the precursors. Liu et al [39] also investigated the simultaneous production of CNTs and hydrogen using a two stage process. PP was pyrolysed and the products then condensed to remove any liquids. The gases were then passed over a NiO catalyst where deposition of CNTs took place. CNTs and hydrogen gas were simultaneously produced in sizeable quantities, with hydrogen making up over 70% of the gas stream produced. CNTs can also be produced from the combustion of plastic sources. In a series of studies Gong et al [29-31] produced CNTs and cup stacked CNTs from a polypropylene source, and found that the amount of chlorine used in the process has a strong effect on the CNT morphology. It is suggested that the growth of CNTs from plastic sources is governed by the production of aromatic products on the catalyst surface.

This study will investigate the key role of steam injection on the production of CNTs and hydrogen from plastic feedstocks. To our knowledge this is the first study to consider the

effect of variation of the steam injection rate on CNT production from plastics. A two stage pyrolysis-gasification process was used where pyrolysed gases were passed directly to a second gasification stage. The effect of the steam injection rate on the quantity and quality of CNTs was investigated. The advantage of this process is that it simultaneously produces carbon nanotubes and hydrogen, and the addition of steam to the system enables larger yields of both products. This means it increases the economic benefit of plastics gasification which was originally only used for hydrogen production. Whilst many studies have considered PE and PP feedstocks for CNT production [27, 32, 37, 38], other plastics such as PS have received less attention. The suitability of the different plastic samples for CNT production will be examined using LDPE, PP and PS.

2 Materials and methods

Polypropylene (PP) was obtained as 2 mm virgin polymer pellets provided by BP Chemicals UK. Low density polyethylene (about 2 mm) (LDPE) and polystyrene (about 2 mm) (PS) were obtained from ACROS Organics UK.

A Ni/Al₂O₃ catalyst was prepared by an impregnation method, with a nickel loading of 5%. Ni(NO₃)₂·6H₂O, deionised water and gamma Al₂O₃ were used as the raw materials. The desired amount of Ni(NO₃)₂·6H₂O was mixed in deionised water and heated at 80°C until dissolved, at which point the Al₂O₃ was added. This mixture was then left to mix until it formed a slurry. This was then dried overnight in an oven at 105°C to remove the remaining water before calcination at 500 °C in an air atmosphere for 3 h. The catalysts were then crushed and sieved to give granules of between 0.065 and 0.212 mm. To characterise the catalyst, BET surface area and XRD analyses were undertaken using a Quantachrome Nova 2200 and a Philips PW 1050 Goniometer, using a PW 1730 with a CuK radiation X-ray tube, respectively. The fresh catalyst had a surface area of 145 m²/g.

The experimental system consisted of a two-stage pyrolysis-gasification reactor as shown in Figure 1. The reactor was made of stainless steel and had a total length of 320 mm and an internal diameter of 22 mm. In each experiment 1 g of the plastic sample was placed inside a sample boat and pyrolysed in first reactor, where the temperature was heated to 600 °C. The generated gaseous products were then passed through to the second reactor, held at 800 °C, and passed over 0.5g of a Ni-Al₂O₃ catalyst allowing hydrogen to be produced with carbon deposition on the catalyst. Nitrogen was used as the carrier gas with a flow rate of 80 ml min⁻¹. The procedure was to heat the second gasification reactor to the desired temperature, then heat the first reactor to 600 °C at a heating rate of 50 °C min⁻¹ for a total reaction time of 30 minutes. Water was injected at various flow rates into the second reactor via a syringe pump, together with the pyrolysed gases derived from the thermal degradation of the plastic from the first stage reactor. Experiments were carried out for each plastic sample with no steam injection and at steam injection rates of 0.25, 1.90 and 4.74 g h⁻¹ so that the effect of steam on the carbon nanotube and hydrogen yield could be investigated.

The volatile products after the gasification process were passed through two condensers, where any condensed products were collected. The non-condensed gases were collected in a 25 L Tedlar™ gas sample bag. The reproducibility of the reaction system was tested and experiments were repeated to ensure the reliability of research results.

Products analysis

The gases collected in the gas sample bag were analysed by packed column gas chromatography (GC). Hydrocarbons (C₁-C₄) were analysed using a Varian 3380 gas chromatograph with a flame ionisation detector, with an 80-100 mesh Hysep column and nitrogen carrier gas. Permanent gases (H₂, CO, O₂, N₂ and CO₂) were analysed with a separate Varian 3380 GC/TCD, thermal conductivity detector, with two packed columns. A

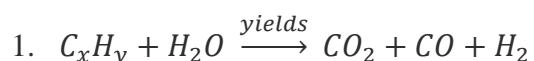
2m long and 2mm diameter column packed with 60-80 mesh molecular sieve was used to analyse hydrogen, nitrogen, carbon monoxide and oxygen. Carbon dioxide was analysed on a 2 m long and 2 mm diameter column with Haysep 60-80 mesh molecular sieve. The carrier gas was argon.

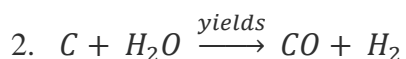
Carbon deposition on the catalyst was analysed by a range of techniques. High resolution scanning and transmission electron microscopy was undertaken using a SEM, LEO 1530 and TEM, FEI Tecnai TF20, to characterise the nature of the carbon that was deposited on the surface of the catalysts during the experimental procedure. The reacted catalysts were analysed by temperature programmed oxidation to investigate the types and relative amounts of carbon deposits on their surfaces. Around 15 mg of the reacted catalyst was heated in a thermogravimetric analyser in an atmosphere of air at a heating rate of 15 °C/min up to a temperature of 800 °C and with a hold time of 10 minutes. Raman spectroscopy was undertaken on the carbon deposits on the catalyst surface to determine their graphitic quality. Results were obtained using a Renishaw Invia Raman spectrometer at a wavelength of 514 nm at Raman shifts between 100 and 3200 cm^{-1} .

3 Results

3.1 Hydrogen production

Table 1 shows the mass balances in terms of the amount of gases, oils and solids produced. The mass balances obtained were all above 93%. For all three samples as the flow rate of steam injected into the reactor was increased, the amount of oils and solids decreased, whilst the amount of gases increased. This is to be expected as steam reforming reactions produce larger amounts of gas, at the expense of oils and solids via equations 1 and 2.





This is also in agreement with results from Erkiaga et al [8] who found that increasing steam/plastic ratio gave a reduction in tars and chars and an increase in gas production, particularly hydrogen. The composition of the gases produced from the plastics samples are shown in Table 1, and are typically composed of H₂, CO, CO₂, CH₄ and C₂-C₄ hydrocarbons. For each of the plastics, hydrocarbons decreased and CO and CO₂ increased via the reaction in equation 1 as the steam injection rate was raised. The higher concentration of CO relative to CO₂ seen is due to the high temperatures used being unfavourable for the water gas shift reaction. To increase the hydrogen yield further a third stage could be employed to convert CO into CO₂ and H₂ via reaction with water. Hydrogen production for each of the plastics is also shown in Table 1 and shows how, as expected by equations 1 and 2, the yield obtained increases with increasing steam injection rate.

The largest gas yields were obtained for LDPE and reached over 80 wt% for a steam injection of 4.74 g h⁻¹ as can be seen in Table 1. Wax was produced at the low steam injection rates, particularly at 0 steam injection, accounting for the large solid yields observed. The hydrogen content of the gas ranged between 50Vol.% and 58Vol.% depending on the steam injection rate as shown in Table 1. A reduction in the content of hydrogen is seen when steam is injected (equations 1 and 2), however in actual terms the amount of hydrogen produced from the plastic is increased, as can be seen in Table 1. Based on its elemental composition the maximum achievable hydrogen production for 100g of LDPE is 41.2g if the hydrogen and carbon in the sample is fully converted to H₂ and CO₂. The maximum hydrogen yield obtained from LDPE at 4.74 g h⁻¹ steam injection was of 9.2 g/100g of sample, roughly 22% of the maximum theoretical yield.

PP also gave high gas yield, as detailed in Table 1, with wax also being produced at lower steam injection rates. The content of hydrogen in the gas is slightly lower than was observed for LDPE and remains around 50vol.% irrespective of the steam injection rate. The maximum hydrogen yield obtained was again achieved with the highest steam injection rate and had a value of 6.9 g/100g sample, lower than was obtained for LDPE. This is roughly 17% of the maximum theoretical yield possible of 41.5g, based on full conversion to H₂ and CO₂. This shows that less of the PP sample was converted into hydrogen than was the case with LDPE. The amount of methane and C₂-C₄ hydrocarbons was also higher than was obtained for LDPE.

Unlike LDPE and PP, PS produced a larger oil yield and smaller proportion of gases as can be seen in Table 1. Enicar and Gonzalez [40] also undertook pyrolysis of various plastics and found that polystyrene gave higher oil yields and lower gas yields than PP and LDPE. PS also shows a comparatively higher hydrogen content in the gas phase compared with PP and LDPE, with values of up to 77vol.% obtained, as seen in Table 1. This is due to the proportion of hydrocarbons in the gas stream being significantly lower than was observed for the other samples, with C₂-C₄ hydrocarbons particularly less abundant. The maximum hydrogen yield obtained with PS was at 4.74 g h⁻¹ steam injection and had a value of 7.4 g/100g sample, roughly 19% of the maximum theoretical yield of 39.0% based on full conversion to H₂ and CO₂.

XRD diffraction plots of the fresh catalyst and used catalysts from PP experiments with and without steam injection are found in Figure 2. The fresh catalyst shows the presence of alumina, and nickel oxide with a particle size of around 5 to 10 nm. The used catalyst without steam instead shows peaks for Ni as opposed to NiO, and has larger particle sizes of around 50 to 100 nm. This suggests that hydrogen produced during the process reduces the NiO to Ni, and that sintering of the Ni particles occur as a result of the high temperature. The

presence of a peak at 26° is also suggestive of a graphitised carbon build up on the catalyst surface. The XRD plot for the used catalyst when steam is injected at a rate of 4.74 g h^{-1} shows a similar profile to that of the used catalyst without steam, with nickel and alumina peaks observed. A marked difference between the two is the lack of a peak representing carbon on the surface, suggesting carbon has reacted with the steam injected.

3.2 Carbon deposits

The solid carbons deposited on the surface of the catalyst were analysed by a range of techniques including SEM, TEM, TPO and Raman spectroscopy.

3.2.1 Low Density Polyethylene

For LDPE scanning electron microscopy images of the carbon deposits obtained at different steam injection rates are shown in Figure 3. Figure 3 (a) shows the deposits on the catalyst surface with no steam injection are predominantly filamentous type carbons. There was a dense covering of these carbons, which were fairly long and thin. When steam was added to the reactor, the SEM images shown in Figure 3 (b) for 0.25 g h^{-1} steam injection continue to show long thin filamentous type carbons. However they were not as densely covered across the catalyst surface due to steam reacting with the carbons on the catalyst surface.

As the steam rate was increased further to 1.90 g h^{-1} and 4.74 g h^{-1} the SEM images in Figures 3 (c) and (d) show fewer carbon deposits. At 1.90 g h^{-1} steam injection, the filamentous carbons are shorter and much more sparsely spread across the catalyst surface and when the steam injection rate was increased further to 4.74 g h^{-1} , there were no filamentous carbon deposits on the catalyst surface. The increased amount of steam appears to have completely reacted with all carbon deposits. The increase in H_2 production observed at the higher steam injection rates is likely to be a result of steam reacting with carbon deposits, as seen in equation 2.

Transmission electron microscopy was also undertaken on the used catalysts to further examine the nature of the carbon deposition on the catalyst surface. Figures 4 (a-h) show the carbon deposits formed from LDPE with varying steam injection rates. Multi walled carbon nanotubes were confirmed which were between 10 and 20 nm in diameter. With no steam injection TEM images in Figures 4 (a) and (b) show that large bundles of these carbon nanotubes were produced. As the steam injection rate is increased to 0.25 g h⁻¹, 1.90 g h⁻¹ and 4.74 g h⁻¹ Figures 4 (c) and (d), (e) and (f) and (g) and (h) respectively show how the amount of carbon nanotubes produced is reduced as seen in the SEM images (Figure 2). In Figures 4 (g) and 3(h) for the steam injection rate of 4.74 g h⁻¹ only a small number of CNTs are observed whereas none were seen from SEM. The nature of the CNTs appears to stay fairly similar irrespective of steam injection, with irregularities and deformities in the CNT structure apparent at all steam rates, and the CNT diameters remaining fairly stable. The length of the carbon nanotubes obtained varies with the rate of steam injection. SEM images in Figures 3 (a), (b), (c) and (d) show that with no steam injection the CNTs are on the μm scale, around 2-4 μm, but when the steam injection is increased the number of longer CNTs drops to the point where none are observed at 4.74 g h⁻¹.

In order to better determine the relative amounts of different types of carbon on the catalyst surface temperature programmed oxidation was carried out on the used catalyst samples. TPO plots for the carbon deposits obtained from LDPE can be seen in Figure 5 (a), with the corresponding derivative plots seen in 5 (b). Figure 5 (a) shows how increasing the amount of steam added into the reactor leads to a reduction in the amount of carbon on the catalyst surface. This correlates with what was seen from SEM and TEM images seen in Figures 3 and 4 respectively, as higher steam injection rates gasified the carbon deposits.

The derivative TPO plots in Figure 5 (b) show two distinct peaks, one at around 540 °C, and another at about 650 °C. Amorphous carbons are reported to show a peak at lower

temperatures than filamentous carbons, due to being more reactive [41]. When no steam is injected the peak associated with the filamentous carbons is large, however the addition of water into the reactor sees this peak become smaller. This is in accordance with the SEM results in Figure 3 where a reduction in the amount of filamentous carbons was observed, as steam reacts with carbon deposits via equation 2. Further increasing the steam injection rate sees a reduction in the size of the peak associated with filamentous carbons, until 4.74 g h^{-1} where virtually none are produced. Table 2 shows the amount of filamentous carbons produced from LDPE, as a weight per cent of the plastic sample. These were calculated from the TPO results and are indicative of CNT production, as CNTs are a type of filamentous carbon. Results show that the yield of filamentous carbons reduces from 18.8% wt to 0% wt as steam injection is increased. As a result the ratio of filamentous:amorphous carbons, also shown in Table 2, reduces from 2.30 to 0.

Raman spectroscopy was also undertaken to characterise the carbon deposits produced, with the spectrum for LDPE shown in Figure 6. Peaks are seen at 1589 cm^{-1} and 1348 cm^{-1} . The peak at 1589 cm^{-1} corresponds to the G peak associated with graphitic carbon structures within the sample, including carbon nanotubes, whilst the peak at 1348 cm^{-1} corresponds with the D peak and is associated with defects within the graphitic lattice or amorphous carbons [42]. For LDPE at 0 steam injection, Figure 6 (a) shows that large G and D peaks are observed and that the G peak is significantly larger than the D peak. This suggests a high purity of CNTs since more graphitic carbons are produced than amorphous carbons or defects in the graphitic structure. Figure 6 (b) shows that once steam is injected the size of the peaks reduce, particularly the G peak. Higher steam injections of 1.90 g h^{-1} and 4.74 g h^{-1} as shown in Figures 6 (c) and (d) see the size of the peaks significantly reduced as carbon deposits are reduced further by increased gasification.

The ratio between the size of the G peak and D peak can be used to compare the quality of the carbon deposits obtained in terms of how ordered and graphitic they are [43-45]. This will enable the purity of the CNTs produced to be evaluated, with a larger G/D ratio indicating a higher purity. For LDPE, the addition of water was detrimental to the purity of CNTs, with a significant decrease observed. A large G/D ratio of over 1.7 was obtained with no steam injection, falling to 1.0 once steam was added.

3.2.2 Polypropylene

SEM images obtained using PP as a feedstock can be seen in Figure 7. Similarly to the images for LDPE, long thin filamentous carbons can be observed along with amorphous carbon deposits. With no steam injection filamentous deposits produced from PP appear not as abundant as was seen with LDPE. When a steam injection 0.25 g h^{-1} was applied, the amount of filamentous carbons appears to remain fairly similar. Raising the steam injection rate further to 1.90 g h^{-1} , 7 (c), and 4.74 g h^{-1} , 7 (d), however sees a clear reduction in the amount and length of the filamentous carbons. As with LDPE the CNTs at no steam injection and 0.25 g h^{-1} are on the μm scale, but at higher steam injection the length reduces, as can be seen in Figures 7 (a), (b), (c) and (d). This again suggests that at these higher steam injection rates, gasification of filamentous carbons occurs. This also accounts for the increased hydrogen and carbon monoxide production observed as steam injection increases.

Figures 8 (a) to (h) show the TEM images of the carbon deposits obtained from the PP feedstock. Similarly to the deposits from LDPE the images show that CNTs are produced for steam injection rates of 0, 0.25 and 1.90 g h^{-1} . Similar diameters between around 10 and 20 nm were also obtained for the CNTs produced from PP feedstock as was found with other plastics. As the steam injection rate was increased the relative amount of CNTs decreases, to the point where at a steam injection rate of 4.74 g h^{-1} (Figures 8 (e) and (f)), only carbon

filaments rather than nanotubes were observed. This is suggestive of a change in growth mechanism at higher steam injection rates.

TPO results for the PP feedstock are shown in Figure 5 (c), with the corresponding derivative plots shown in Figure 5 (d). Similarly to LDPE the TPO plots in Figure 5 (c) show how, as the steam injection rate is increased the amount of carbon oxidised from the catalyst surface was reduced as suggested by the SEM and TEM results (Figures 7 and 8 respectively).

The derivative plots show similarities to those obtained from LDPE, with two distinct peaks observed, again representing amorphous and filamentous carbons. The amount of filamentous carbons produced is shown in Table 2. Contrary to what was seen with LDPE a small increase is seen from 8.8% wt to 10.4% wt as steam is added. The ratio of filamentous to amorphous carbons increases from 0.44 to 0.89, suggesting that the amount of amorphous carbons has reduced. At higher steam injections filamentous carbon production falls to 3%, leading to the filamentous:amorphous ratio falling to 0.33. At 4.74 g h⁻¹ the filamentous:amorphous ratio raises again to 0.57, as the amount of amorphous carbons reduce.

Raman spectra for the carbon deposits obtained from PP are shown in Figures 9 (a) to (d) and show a similar pattern as was seen with LDPE. For all the spectrums D and G peaks are observed, with larger peaks observed at low steam injection and significantly smaller peaks seen at steam injections of 1.90 g h⁻¹ and 4.74 g h⁻¹. The relative height of the G peak compared to the D peak reduces when steam is introduced suggesting that, as was seen with LDPE, the amount of ordered graphitic carbon decreases, and with it the purity of the CNTs. This would suggest that whilst an increase in the amount of filamentous carbons was observed for PP at 0.25 g h⁻¹ steam injection, the purity of the CNTs is low. At 4.74 g h⁻¹ the D band is actually larger than the G band, which suggests the deposits are more disordered, which is in agreement with the TEM images in Figure 8, since a larger proportion of

filaments were seen in comparison to CNTs. The injection of steam into the system sees a decrease in the G/D ratio, falling from 1.2 to 1.0, indicating the purity of the carbon deposits has decreased.

3.2.3 Polystyrene

The SEM images of the carbon deposits from the PS samples, seen in Figure 10, show long thin filamentous carbons similar to those seen from the other plastic samples. The 0 and 0.25 g h⁻¹ steam injection rates show a much larger amount of the long thin filamentous deposits associated with carbon nanotubes than can be seen in Figures 10 (c) and (d) for steam injections of 1.90 and 4.74 g h⁻¹. The deposits at the higher steam injection ratios do however show more carbon deposits than those obtained from the other plastics, but the nature of the filamentous carbons are much thicker and shorter, and more likely to be the carbon filaments rather than CNTs. The length of the CNTs obtained at no steam injection and 0.25 g h⁻¹ are comparable to those seen with the other plastic samples, on the μm scale. At higher steam injection rates, some CNTs are still of a μm length, but tend to be shorter at around 1 to 2 μm as opposed to the 3 to 4 μm seen at low steam injection rates as can be seen in the SEM images in Figures 10 (a), (b), (c), and (d).

The TEM images of the carbon deposits from PS in Figures 11 (a) to (h) show that multiwalled CNTs are also produced from this feedstock. At 0, 0.25 and 1.90 g h⁻¹ steam injection the CNTs have diameters of around 10-20 nm as was seen with the other plastics, with some larger diameters also produced, as is seen in Figures 11 (a) to (f). When the steam injection rate was increased to 4.74 g h⁻¹ however, there were very few CNTs observed, with amorphous and filamentous carbons being the predominant deposits. The nanotubes that were observed had a very large diameter, as seen in Figures 11 (g) and (h).

For PS the TPO results are particularly interesting, with Figures 5 (e) and (f) showing that unlike the results seen for LDPE and PP, there is actually an increase in the amount of carbon deposition on the surface on the catalyst at a steam injection rate of 0.25 g h^{-1} . At steam rates beyond this the amount of carbon deposition once again drops as witnessed with the other plastic samples. The derivative plot, Figure 5 (f), reveals that the type of carbon produced at 0.25 g h^{-1} is predominantly filamentous carbon such as carbon nanotubes, along with a small amount of amorphous carbons. The amount of amorphous carbons produced is less than was observed for 0 steam injection and remains low for the other steam injection rates.

Table 2 shows that the amount of filamentous carbons produced from PS first increases when 0.25 g h^{-1} of steam is added up to 32% wt, before reducing at the higher steam injection rates to 7%. The ratio of filamentous:amorphous carbons at 0.25 g h^{-1} is high, at a value of 4.47. It then shows a similar pattern to PP, with a reduction seen to 0.49 at 1.90 g h^{-1} as filamentous carbons reduce, and then an increase to 0.92 as amorphous carbons are destroyed.

Raman spectra obtained for the carbon deposits from PS can be seen in Figures 12 (a) to (d). As with the spectrums obtained from LDPE and PP, G and D peaks are observed, with the relative heights of these varying with the steam injection rate. At 0 and 0.25 g h^{-1} steam injection, (Figures 12 (a) and (b) respectively) the peaks observed are large, but for PS it can be seen that height of the G peak to the D peak actually increases when 0.25 g h^{-1} of steam is injected. This contrasts with the results obtained from the other plastic feedstocks where the injection of steam results in a significant reduction in the relative height of the G peak. The rise in this instance is likely due to the large increase in the amount of CNTs produced at this steam injection rate, giving more graphitic carbon.

4 Discussion

4.1 Effect of steam on carbon deposition

Overall, increasing the amount of steam had the effect of reducing the amount of carbon deposits. This is in agreement with the reduction in solid yields observed in Table 1, as steam reacts with carbon deposits to produce CO and H₂ (equation 2). TPO analyses for each of the carbons, seen in Figure 5, show how the amount of total carbon deposition on the catalyst surface decreases as more steam is injected. This is true for each of the plastics with the exception of PS at 0.25 g h⁻¹, which will be discussed later.

Furthermore, increasing the steam injection rate appears to also reduce the amount of filamentous carbons produced, with SEM images in Figures 3, 7 and 10 showing the smallest amount observed at steam injection rates of 4.74 g h⁻¹. It is reported by Figueiredo and Trimm [46] that the gasification of filamentous carbons, such as CNTs, occurs as the reverse of their formation mechanism, and that the rate of gasification is independent of the amount of carbon deposited on supported catalysts. This would suggest that CNTs are formed when the rate of gasification of the deposited carbons is less than the rate of formation. As steam is injected into the reactor, the rate of gasification will increase, and result in the reduction in the yield of filamentous carbons observed. The gasification of these carbon deposits would also account for the increase in hydrogen and carbon monoxide levels at higher steam injection rates as seen in Table 1. When undertaking steam reforming of a model bio-oil compound Wu and Liu [47] found similar results, with increased steam injection leading to a decrease in filamentous carbons produced.

Another effect that steam has on carbon deposits is an increase in the formation of CNTs by increased activity of the catalyst, as a result of destruction of amorphous carbons [26]. For PP and PS at 0.25 g h⁻¹ steam injection TPO results seen in Table 2 shows an increase in the

amount of filamentous deposits produced. Derivative plots shown in Figure 4 also show that the addition of steam into the reactor leads to a reduction in amorphous carbons. This suggests that the effect of increased CNT production by increased catalytic activity outweighs the effect of steam disrupting the production of CNTs. So whilst less filaments may be formed, since some are gasified, where they are produced the higher activity of the catalyst leads to an overall increase in CNT production.

At injection rates beyond 0.25 g h^{-1} however Table 2 shows a reduction in the yield of filamentous carbons obtained for each of the plastics. This suggests that more formation of CNTs are prevented by steam inhibition than enabled by increased catalyst activity, leading to a reduction in the overall production of CNTs. This suggests that the variation of steam is a key attribute to CNT growth, and that whilst the optimum amount can lead to an increase in the yield, too much steam prevents CNT production. From our results steam injection rates of 1.90 and 4.74 g h^{-1} have shown to be clearly unsuitable for CNT production in this work.

From the TEM analyses of PP and PS, shown in Figures 8 and 11, it can be seen that there is a change in the type of carbon deposits which occur with an increase in steam injection. Whilst CNTs are produced at low steam injection rates, at higher steam injection, and particularly at 4.74 g h^{-1} carbon fibres without a hollow central channel are seen. Snoeck et al [48] suggest that the difference in formation of carbon fibres and CNTs is due to the different rate at which carbon deposition nucleates compared to the diffusion through the nickel catalyst. When carbon deposition occurs slower it is more likely to form fibres, whilst fast deposition form CNTs since deposition is fast compared to diffusion, meaning it only occurs around the particles edge, forming a tube. A similar mechanism could explain why carbon fibres are formed rather than CNTs at high steam injection rates, since the rate of carbon formation could be slowed due to the presence of steam.

Steam injection has shown to be of crucial importance to both the production of hydrogen and CNTs. However, the maximum yields of each occur at different steam injection rates. Low steam injection rates of 0 g h^{-1} and 0.25 g h^{-1} proved most productive for CNT production, whilst the highest hydrogen yields were obtained at 4.74 g h^{-1} . This gives the potential for an industrial process which has great flexibility over its production, where by simply changing the steam injection rate the major product can be switched between hydrogen and CNTs.

4.2 Effect of plastic type on carbon deposition

The plastics pyrolysis products affinity to produce filamentous carbons and amorphous carbons had a strong bearing on their CNT production at different steam injection rates. Whilst SEM and TEM images in Figures 3, 4, 7, 8, 10 and 11 showed that CNTs were produced from each plastic, there are differences in the relative abundances of both CNTs and amorphous carbons produced from the different feedstocks. Without steam injection Table 2 shows that LDPE produced 19% wt of CNTs, much larger than either PP, 9% wt, or PS, 10% wt.

It is likely that more CNTs are formed from LDPE since a comparatively small amount of amorphous carbons were seen with this feedstock, with a filamentous:amorphous ratio of 2.30 compared with 0.44 for PP and 0.46 for PS, as shown in Table 2. This would allow more CNT production from LDPE, whilst PP and PS which produce more amorphous carbons would see CNT growth restricted by deactivation of the catalyst. Accordingly results from Raman spectroscopy showed that LDPE had a much higher purity of CNTs with a G/D ratio of 1.7, compared with 1.2 for PP and 1.1 for PS. Amorphous carbons could be higher for PP and PS as a result of larger hydrocarbons being produced from these feedstocks. This

correlates with the results shown in Table 1, which show that PP gave a larger amount of C₂-C₄ hydrocarbons, whilst PS gave a much bigger yield of larger oil compounds.

Once steam is injected at 0.25 g h⁻¹, significant changes are observed. The results in Table 2 now show that whilst LDPE shows a reduction in the amount of filamentous carbons, to 8% wt, PP and PS see increases to 10% wt and 32% wt respectively. The addition of steam has two effects on the production of filamentous carbons, one is to increase the formation of CNTs by increased activity of the catalyst, as a result of destruction of amorphous carbons [26]. The other is the destruction of CNTs by gasification.

For PP and PS at 0.25 g h⁻¹ steam injection it suggests that the effect of increased CNT production by increased catalytic activity outweighs the effect of steam disrupting the production of CNTs. This was not true for LDPE. For PP this could be due to the fact that it forms larger molecules when pyrolysed than LDPE. The gas composition in Table 1 confirms more C₂-C₄ hydrocarbons are produced from PP. Rostrup-Nielsen found that larger molecules form more filamentous carbons [49], and since gasification is independent of the amount of carbon, gasification of these filaments will leave a higher proportion for PP than for LDPE. Increased filamentous carbons found for PS is likely due to the fact that aromatic precursors form more filamentous carbons than olefins [49]. This is also in accordance with the mechanism for production of CNTs from plastics as proposed by Gong et al, who suggested that CNTs are produced from polymerisation of aromatics compounds on the catalyst surface [29]. PS is an aromatic based polymer and would form more aromatics on the catalyst surface than the olefinic plastics.

Raman spectroscopy results for PS, showed an increase in the G/D ratio as the purity of CNTs increased. For PP a reduction in G/D ratio was observed, however the increase in filamentous carbon production for this feedstock was very small. This suggests that at 0.25 g h⁻¹ for PP the reduction in the G/D band could be a result of filamentous carbons rather than

CNTs being produced. For LDPE a significant reduction in the G/D ratio is seen, from 1.7 to 1.0, concurrent with the reduction in CNT purity as less are produced.

For the higher steam injection rates of 1.90 and 4.74 g h⁻¹, PP and LDPE produced similar results with reductions in the amounts filamentous carbons observed from SEM, in Figures 3, 7 and 10, and from TPO in Table 2. For a steam injection rate of 4.74 g h⁻¹ the filamentous carbon production was severely depleted with values of 0.0 and 3.4 wt.% shown for LDPE and PP respectively. This would suggest that these high steam injection rates are unsuitable for CNT production from olefinic hydrocarbons, as the ratio of steam to carbon is too high and simply results in a reaction between the two. Whilst TPO results for PS in Table 2 show that the amount of filamentous carbons reduced at the higher steam injection rates, more are produced than was observed for LDPE and PP with a value for PS of 7 wt.% at 4.74 g h⁻¹. Jackson et al [50] similarly reported that whilst olefinic feedstocks such as pentane and hexane resulted in the production of filamentous carbons disappearing at high steam injection rates, aromatic sources such as benzene, toluene and ethyl-benzene continued to show production of filamentous carbons. In this work, as PS is an aromatic based polymer when the pyrolysis products from the first stage pyrolysis step reach the catalyst they will behave in a manner similar to the aromatic sources used by Jackson et al.

5 Conclusions

The pyrolysis-gasification of plastics has shown that the production of hydrogen was increased when the steam injection rate was increased. This is ascribed to a combination of increased steam reforming reactions, and also gasification of carbon deposits on the catalyst surface. LDPE produced roughly 20% of the maximum theoretical hydrogen yield, with the

relative productions of, LDPE > PS > PP for the percentage of maximum theoretical yield achieved.

With no steam injection LDPE produces a small amount of amorphous carbons and so the catalyst is less readily deactivated and a large number of CNTs are produced. Even though PS and PP have a better affinity to produce filamentous carbons such as CNTs, they also produce more amorphous carbons from large hydrocarbons and so the catalyst is quickly deactivated and less CNTs are produced.

For PS and PP the critical point where the increase in activity of the catalyst outweighs the destruction of CNTs by gasification is reached at 0.25 g h^{-1} since they produce filamentous carbons more readily, leaving a smaller proportion destroyed by gasification. At higher steam injection rates, more CNTs are prevented by gasification and at this point it has a larger effect than the increase in catalytic activity. PS produced the largest yield of filamentous carbons, with 32 wt.% produced from 1g of sample.

Results show that the rate of steam injection is crucial for CNT production. The maximum yields for hydrogen and CNTs occurred at different steam injection rates, since gasification at high injection rates of CNTs gives a higher hydrogen production. Therefore, there is potential for a process with good flexibility over production, where by changing the steam injection rate the major product can be shifted from CNTs to hydrogen.

Acknowledgements

The support from the UK Engineering and Physical Sciences Research Council for a scholarship for one of us (JCA) is gratefully acknowledged.

References

- [1] DEFRA, Municipal Waste Composition: A Review of Municipal Waste Component Analyses, Department for Environment, Food and Rural Affairs 2009.
- [2] P. Europe, Plastics - the Facts 2011: An analysis of European plastics production, demand and recovery for 2010, Plastics Europe, EuPC, EuPR, EPRO, 2011.
- [3] A. Demirbas, *Journal of Analytical and Applied Pyrolysis* 72 (2004) 97-102.
- [4] M. He, B. Xiao, Z. Hu, S. Liu, X. Guo, S. Luo, *International Journal of Hydrogen Energy* 34 (2009) 1342-1348.
- [5] Y. Kodera, Y. Ishihara, *Energy & Fuels* 20 (2006) 155-158.
- [6] I.I. Ahmed, A.K. Gupta, *International Journal of Hydrogen Energy* 34 (2009) 6253-6264.
- [7] S. Czernik, R.J. French, *Energy & Fuels* 20 (2006) 754-758.
- [8] A. Erkiaga, G. Lopez, M. Amutio, J. Bilbao, M. Olazar, *Fuel* 109 (2013) 461-469.
- [9] T. Namioka, A. Saito, Y. Inoue, Y. Park, T.-j. Min, S.-a. Roh, K. Yoshikawa, *Applied Energy* 88 (2011) 2019-2026.
- [10] Y. Park, T. Namioka, S. Sakamoto, T.-j. Min, S.-a. Roh, K. Yoshikawa, *Fuel Processing Technology* 91 (2010) 951-957.
- [11] W. Tongamp, Q. Zhang, F. Saito, *International Journal of Hydrogen Energy* 33 (2008) 4097-4103.
- [12] C. Wu, P.T. Williams, *Applied Catalysis B: Environmental* 87 (2009) 152-161.
- [13] C. Wu, P.T. Williams, *Applied Catalysis B: Environmental* 90 (2009) 147-156.
- [14] C. Wu, P.T. Williams, *Fuel* 89 (2010) 3022-3032.
- [15] F. Aupretre, C. Descorme, D. Duprez, *Catalysis Communications* 3 (2002) 263-267.
- [16] J.R. Rostrup-Nielsen, *Steam Reforming Catalysts*, Danish Technical Press, Copenhagen, 1975.
- [17] J.C. Acomb, M.A. Nahil, P.T. Williams, *Journal of Analytical and Applied Pyrolysis* (2012).
- [18] C. Wu, Z. Wang, L. Wang, P.T. Williams, J. Huang, *RSC Advances* 2 (2012) 4045-4047.
- [19] S. Iijima, *Letters to Nature* 354 (1991) 56-58.
- [20] G.D. Nessim, *Nanoscale* 2 (2010) 1306-1323.
- [21] R.T.K. Baker, M.A. Barber, P.S. Harris, F.S. Feates, R.J. Waite, *Journal of Catalysis* 26 (1972) 52-62.
- [22] R.T.K. Baker, P.S. Harris, R.B. Thomas, R.J. Waite, *Journal of Catalysis* 30 (1973) 86-95.
- [23] J.P. Tessonnier, D.S. Su, *ChemSusChem* 4 (2011) 824-847.
- [24] C. Wu, P.T. Williams, *International Journal of Hydrogen Energy* 35 (2010) 949-957.
- [25] H. Ago, N. Uehara, N. Yoshihara, M. Tsuji, M. Yumura, N. Tomonaga, T. Setoguchi, *Carbon* 44 (2006) 2912-2918.

- [26] K. Hata, D.N. Futaba, K. Mizuno, T. Namai, M. Yumura, S. Iijima, *Science* 306 (2004) 1362-1364.
- [27] E.F. Kukovitskii, L.A. Chernozatonskii, S.G. L'vov, N.N. Mel'nik, *Chemical Physics Letters* 266 (1997) 323-328.
- [28] T. Tang, X. Chen, X. Meng, H. Chen, Y. Ding, *Angew Chem Int Ed Engl* 44 (2005) 1517-1520.
- [29] J. Gong, J. Liu, D. Wan, X. Chen, X. Wen, E. Mijowska, Z. Jiang, Y. Wang, T. Tang, *Applied Catalysis A: General* 449 (2012) 112-120.
- [30] J. Gong, J. Liu, L. Ma, X. Wen, X. Chen, D. Wan, H. Yu, Z. Jiang, E. Borowiak-Palen, T. Tang, *Applied Catalysis B: Environmental* 117-118 (2012) 185-193.
- [31] J. Gong, J. Liu, Z. Jiang, X. Wen, X. Chen, E. Mijowska, Y. Wang, T. Tang, *Chemical Engineering Journal* 225 (2013) 798-808.
- [32] L.A. Chernozatonskii, E.F. Kukovitskii, A.L. Musatov, A.B. Ormont, *Carbon* 36 (1998) 713-715.
- [33] N.A. Kiselev, J. Sloan, D.N. Zakharov, E.F. Kukovitskii, J.L. Hutchison, J. Hammer, A.S. Kotosonov, *Carbon* 36 (1998) 1149-1157.
- [34] N.I. Maksimova, O.P. Krivoruchko, G. Mestl, V.I. Zaikovskii, A.L. Chuvilin, A.N. Salanov, E.B. Burgina, *Journal of Molecular Catalysis A: Chemical* 158 (2000) 301-307.
- [35] Y.-H. Chung, S. Jou, *Materials Chemistry and Physics* 92 (2005) 256-259.
- [36] J.H. Zhang, J. Li, H. Cao, Y.T. Qian, *Materials Letters* 62 (2008) 1839-1842.
- [37] V.G. Pol, P. Thiyagarajan, *Journal of Environmental Monitoring* 12 (2010) 455-459.
- [38] N. Mishra, G. Das, A. Ansaldo, A. Genovese, M. Malerba, M. Povia, D. Ricci, E. Di Fabrizio, E. Di Zitti, M. Sharon, M. Sharon, *Journal of Analytical and Applied Pyrolysis* 94 (2012) 91-98.
- [39] J. Liu, Z. Jiang, H. Yu, T. Tang, *Polymer Degradation and Stability* 96 (2011) 1711-1719.
- [40] E. JM, G. JF, *Fuel Processing Technology* 89 (2008) 678 - 686.
- [41] P. Wang, E. Tanabe, K. Ito, J. Jia, H. Morioka, T. Shishido, K. Takehira, *Applied Catalysis A: General* 231 (2002) 34-44.
- [42] Z.W. Jiang, R.J. Song, W.G. Bi, J. Lu, T. Tang, *Carbon* 45 (2007) 449-458.
- [43] N. Das, A. Dalai, J. Soltanmohammadzadeh, J. Adjaye, *Carbon* 44 (2006) 2236-2245.
- [44] W. Qian, *Carbon* 41 (2003) 1851-1854.
- [45] J. Sengupta, A. Jana, N.D. Pradeep Singh, C. Jacob, *Materials Research Bulletin* 45 (2010) 1189-1193.
- [46] J.L. Figueiredo, D.L. Trimm, *Journal of Catalysis* 40 (1975) 154-159.
- [47] C. Wu, R. Liu, *International Journal of Hydrogen Energy* 35 (2010) 7386-7398.
- [48] J.W. Snoeck, G.F. Froment, M. Fowles, *Journal of Catalysis* 169 (1997) 240-249.
- [49] J.R. Rostrup-Nielsen, *Journal of Catalysis* 33 (1974) 184-201.
- [50] S.D. Jackson, S.J. Thomson, G. Webb, *Journal of Catalysis* 70 (1981) 249-263.

Table 1

Mass balance, gas composition and hydrogen yield from the pyrolysis-gasification of LDPE, PP and PS

Sample	LDPE	LDPE	LDPE	LDPE	PP	PP	PP	PP	PS	PS	PS	PS
Steam injection (g h ⁻¹)	0	0.25	1.90	4.74	0	0.25	1.90	4.74	0	0.25	1.90	4.74
Gas (wt %)	30.9	58.8	78.9	85.7	44.8	57.1	69.8	80.3	11.7	23.9	46.4	56.1
Oils (wt %)	14.0	8.2	0.0	0.0	16.0	6.5	8.3	0.0	53.0	37.7	31.0	25.1
Solid * (wt %)	52.0	25.0	15.5	12.5	35.0	30.9	20.0	14.0	35.0	38.4	18.2	12.3
H ₂ (Vol.%)	58.3	50.3	53.8	53.1	51.1	50.0	51.60	49.5	77.2	68.5	64.4	60.0
CO (Vol.%)	0.0	13.1	26.4	21.1	0.0	14.9	18.3	21.6	0.0	16.7	22.2	26.3
CO ₂ (Vol.%)	0.0	0.7	3.1	6.2	0.0	1.0	4.7	6.4	0.0	0.9	6.3	8.2
CH ₄ (Vol.%)	20.3	16.1	7.1	7.1	19.3	13.7	9.0	5.5	12.0	8.5	4.0	2.2
C ₂ -C ₄ (Vol.%)	21.4	19.7	9.7	12.5	29.7	20.4	16.3	17.0	10.7	5.4	3.2	3.2
H ₂ yield (g/100g sample)	3.3	4.7	9.0	9.2	3.3	4.4	6.2	6.9	2.7	3.8	6.9	7.4

*Solid fraction includes carbon deposition, solid residue and waxes obtained after reaction

Table 2

Proportion of filamentous carbons and amorphous produced in carbon deposits and total filamentous carbon production

Plastic	LDPE	LDPE	LDPE	LDPE	PP	PP	PP	PP	PS	PS	PS	PS
Steam injection (g h ⁻¹)	0	0.25	1.90	4.74	0	0.25	1.90	4.74	0	0.25	1.90	4.74
Filamentous carbon production (wt %)	18.8%	7.6%	1.6%	0.0%	8.8%	10.4%	3.3%	3.4%	9.6%	32.4%	6.3%	7.0%
Ratio of filamentous carbons: Amorphous carbons	2.30	0.67	0.23	0	0.44	0.89	0.33	0.57	0.46	4.47	0.49	0.92

Figure captions

1. Schematic diagram of the pyrolysis-gasification reactor
2. XRD analysis of (a) fresh Ni Al₂O₃ catalyst, (b) used Ni Al₂O₃ catalyst with 0 steam injection and (c) used Al₂O₃ catalyst with 4.74 g h⁻¹ steam injection
3. SEM images of carbon deposits obtained from LDPE at steam flow rates of (a) 0 g h⁻¹, (b) 0.25 g h⁻¹, (c) 1.90 g h⁻¹ and (d) 4.74 g h⁻¹
4. TEM images of carbon deposits obtained from LDPE at steam flow rates of (a-b) 0 g h⁻¹ (c-d) 0.25 g h⁻¹, (e-f) 1.90 g h⁻¹ and (g-h) 4.74 g h⁻¹
5. Temperature programmed oxidation plots for LDPE (a), PP (c) and PS (e) and corresponding derivative plots (b), (d) and (f)
6. Raman spectrums for carbon deposits from LDPE with (a) 0 steam injection, (b) 0.25 g h⁻¹ steam injection, (c) 1.90 g h⁻¹ steam injection and (d) 4.74 g h⁻¹ steam injection
7. SEM images of carbon deposits obtained from PP at steam flow rates of (a) 0 g h⁻¹, (b) 0.25 g h⁻¹, (c) 1.90 g h⁻¹ and (d) 4.74 g h⁻¹
8. TEM images of carbon deposits obtained from PP at steam flow rates of (a) 0 g h⁻¹, (b) 0.25 g h⁻¹, (c) 1.90 g h⁻¹ and (d) 4.74 g h⁻¹
9. Raman spectrums for carbon deposits from PP with (a) 0 steam injection, (b) 0.25 g h⁻¹ steam injection, (c) 1.90 g h⁻¹ steam injection and (d) 4.74 g h⁻¹ steam injection
10. SEM images of carbon deposits obtained from PS at steam flow rates of (a) 0 g h⁻¹, (b) 0.25 g h⁻¹, (c) 1.90 g h⁻¹ and (d) 4.74 g h⁻¹
11. TEM images of carbon deposits obtained from PS at steam flow rates of (a) 0 g h⁻¹, (b) 0.25 g h⁻¹, (c) 1.90 g h⁻¹ and (d) 4.74 g h⁻¹
12. Raman spectrums for carbon deposits from PS with (a) 0 steam injection, (b) 0.25 g h⁻¹ steam injection, (c) 1.90 g h⁻¹ steam injection and (d) 4.74 g h⁻¹ steam injection

Figure 1

Schematic diagram of the pyrolysis-gasification reactor

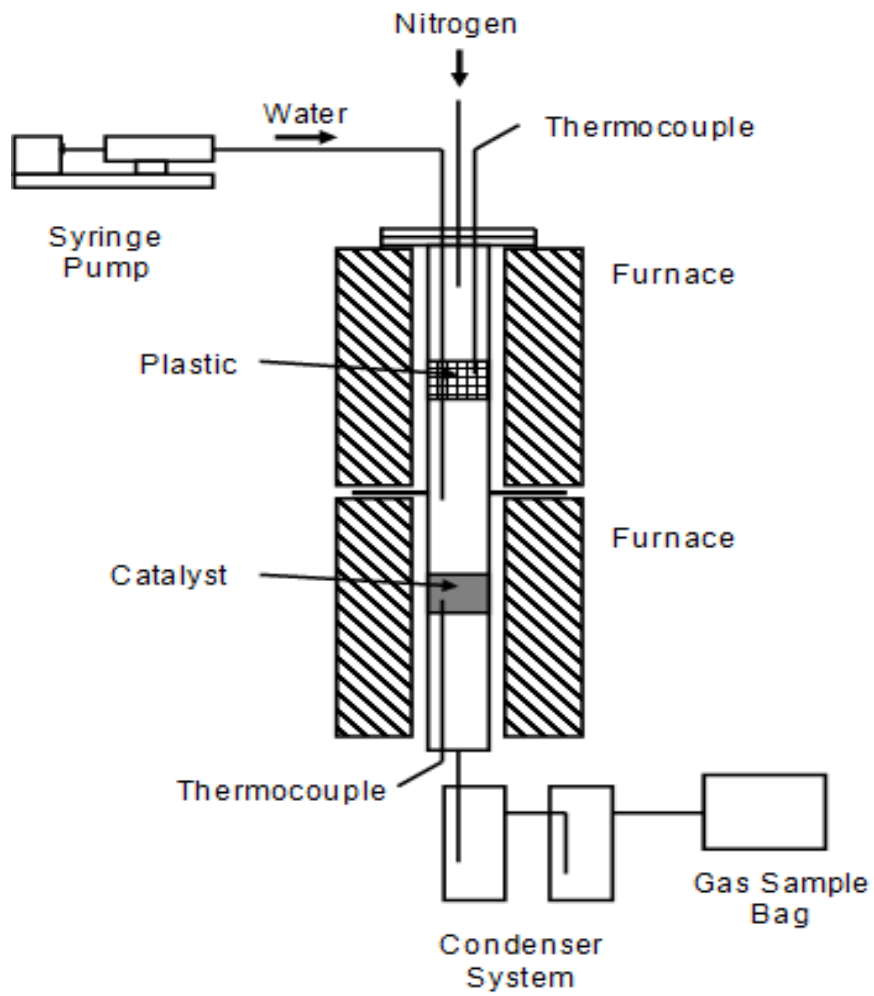


Figure 2

XRD analysis of (a) fresh Ni Al₂O₃ catalyst, (b) used Ni Al₂O₃ catalyst with 0 steam injection and (c) used Al₂O₃ catalyst with 4.74 g h⁻¹ steam injection

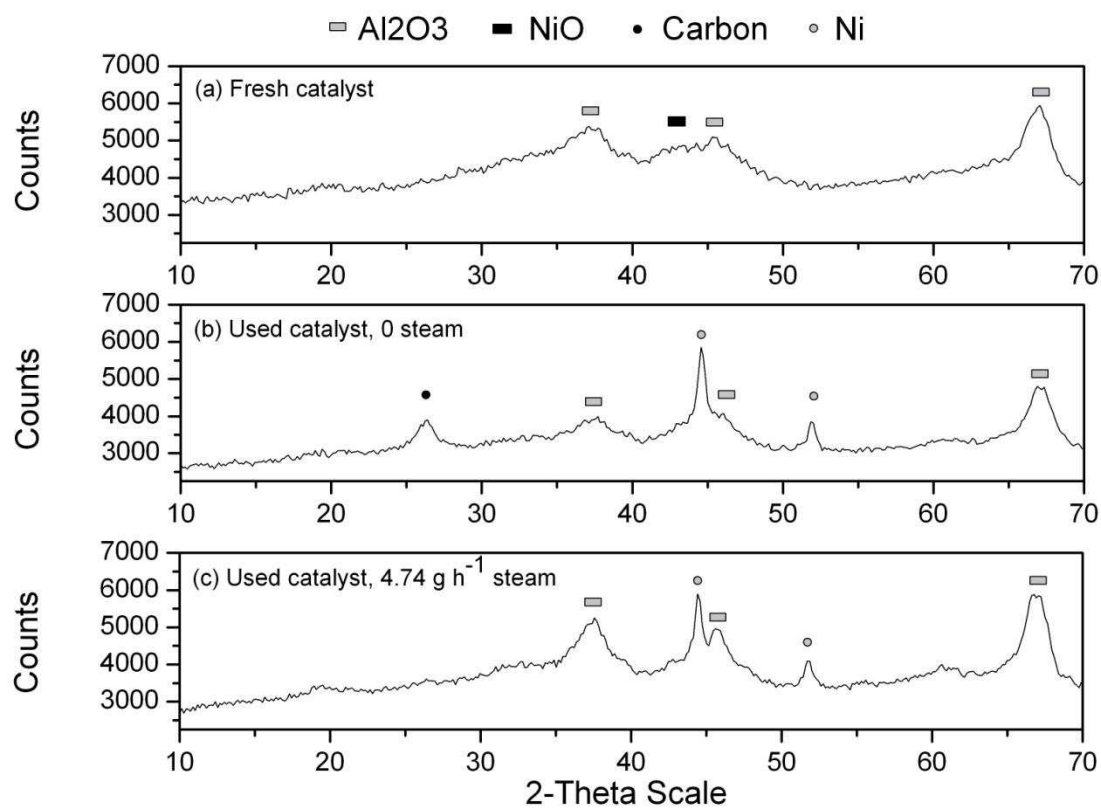


Figure 3

SEM images of carbon deposits obtained from LDPE at steam flow rates of (a) 0 g h^{-1} , (b) 0.25 g h^{-1} , (c) 1.90 g h^{-1} and (d) 4.74 g h^{-1}

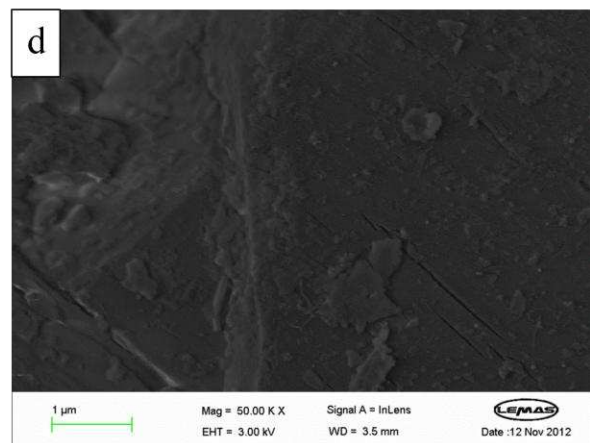
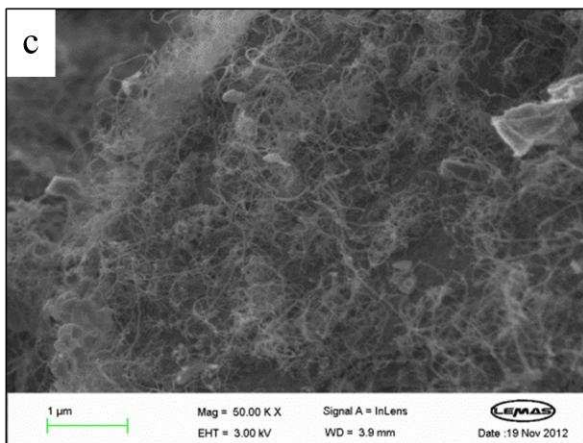
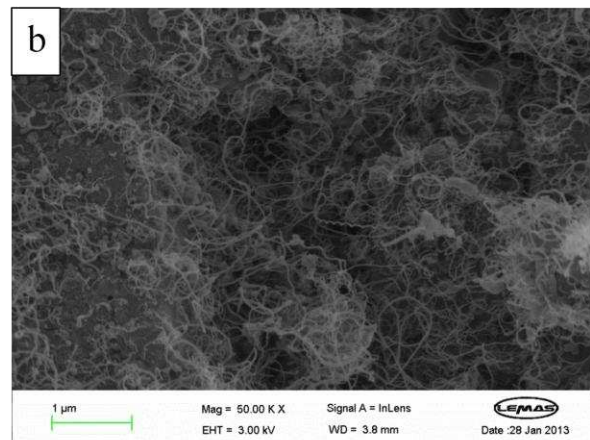
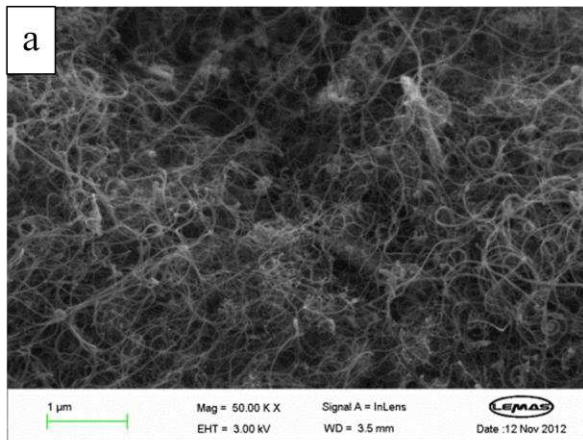


Figure 4

TEM images of carbon deposits obtained from LDPE at steam flow rates of (a-b) 0 g h^{-1} (c-d) 0.25 g h^{-1} , (e-f) 1.90 g h^{-1} and (g-h) 4.74 g h^{-1}

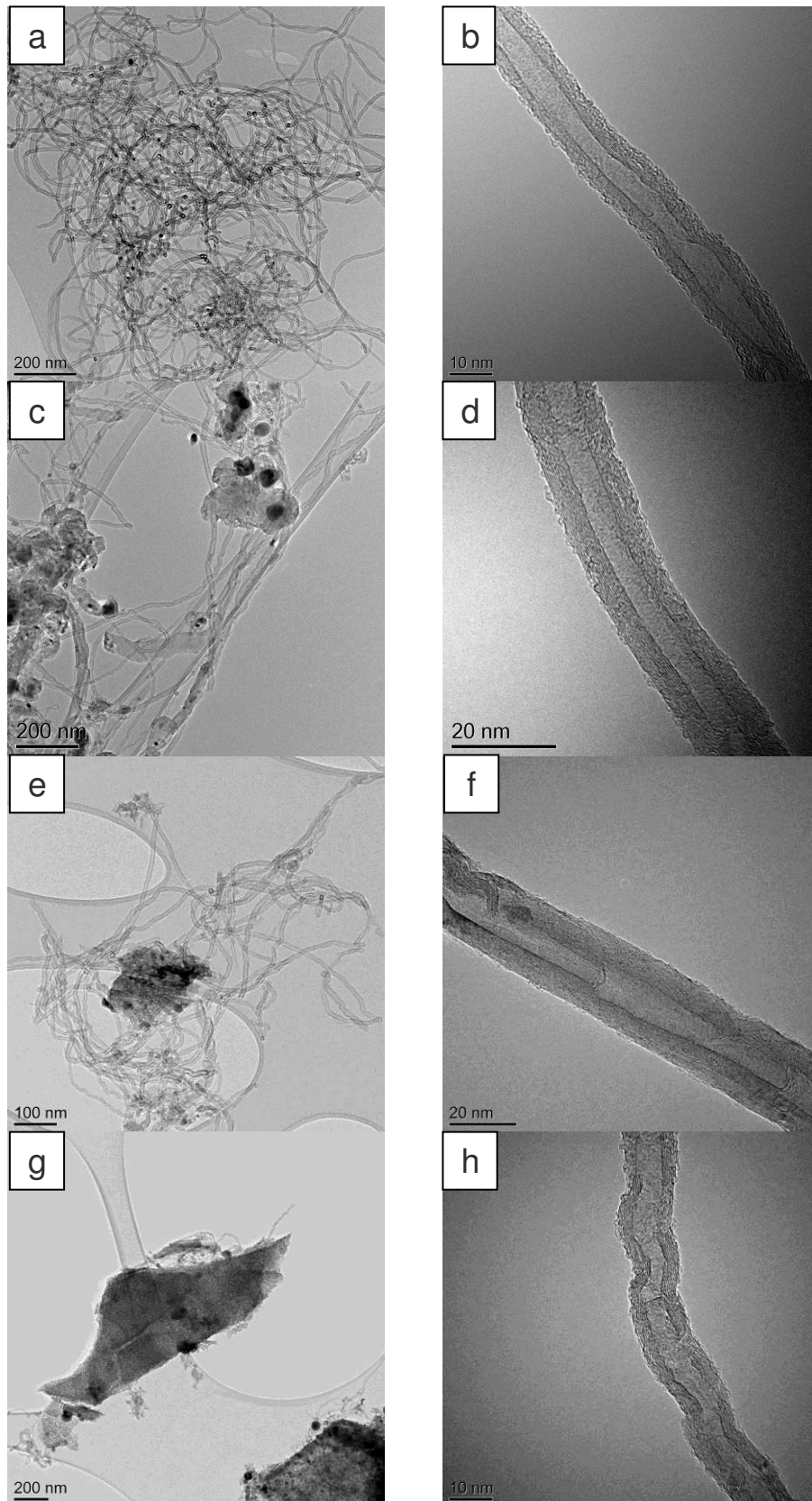


Figure 5

Temperature programmed oxidation plots for LDPE (a), PP (c) and PS (e) and corresponding derivative plots (b), (d) and (f)

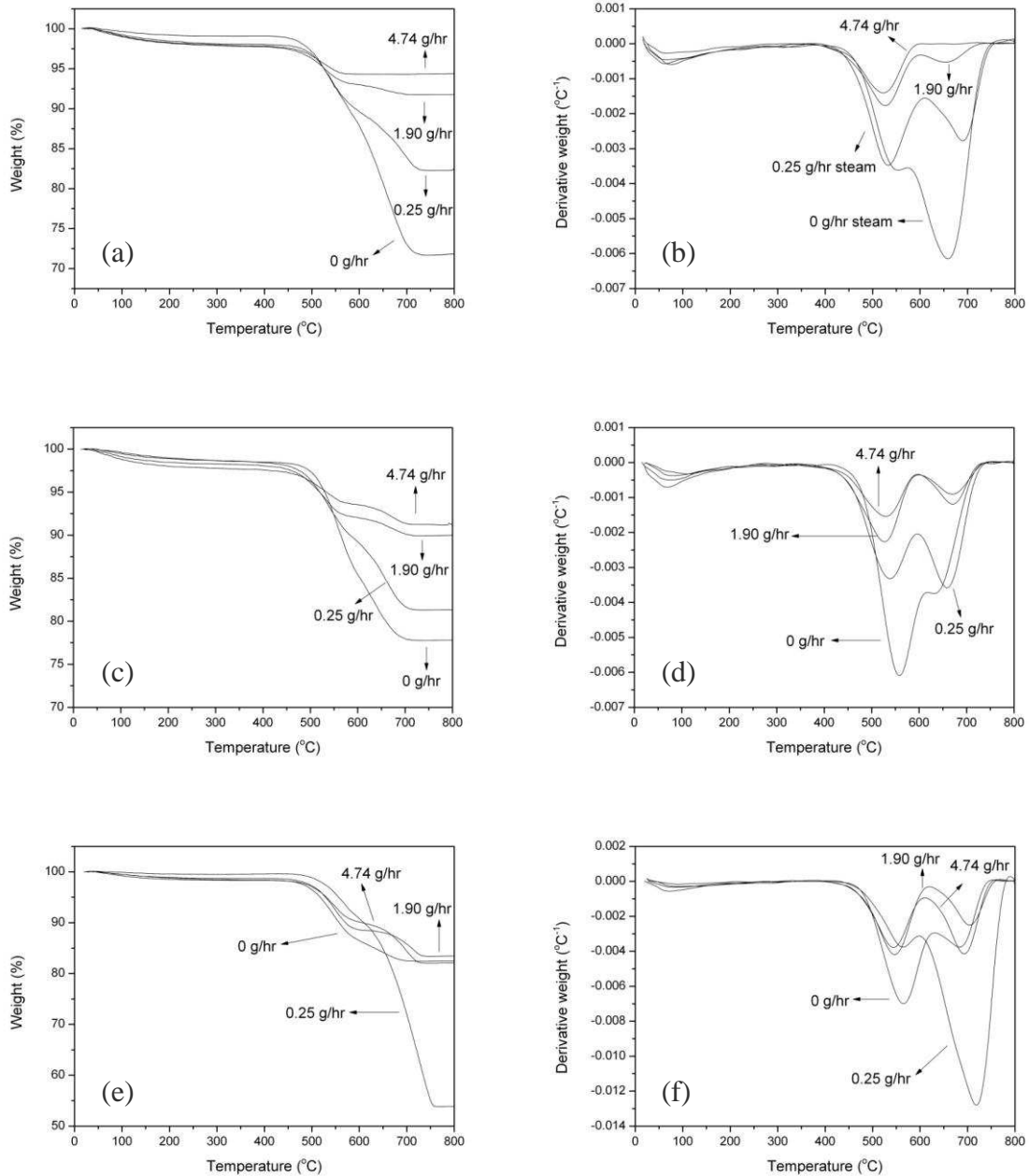


Figure 6

Raman spectrums for carbon deposits from LDPE with (a) 0 steam injection, (b) 0.25 g h^{-1} steam injection, (c) 1.90 g h^{-1} steam injection and (d) 4.74 g h^{-1} steam injection

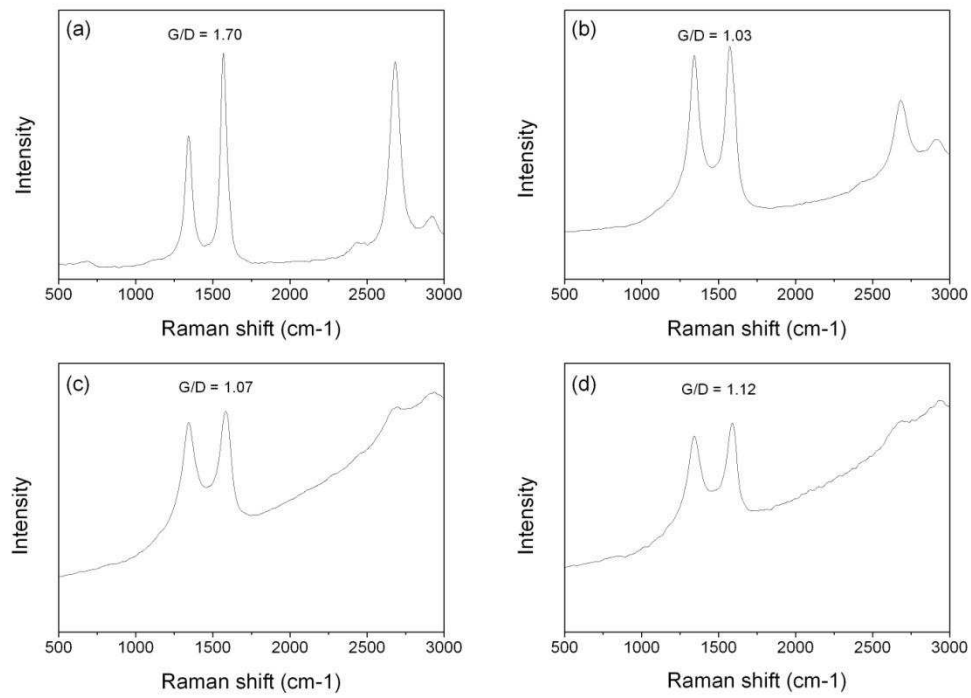


Figure 7

SEM images of carbon deposits obtained from PP at steam flow rates of (a) 0 g h^{-1} , (b) 0.25 g h^{-1} , (c) 1.90 g h^{-1} and (d) 4.74 g h^{-1}

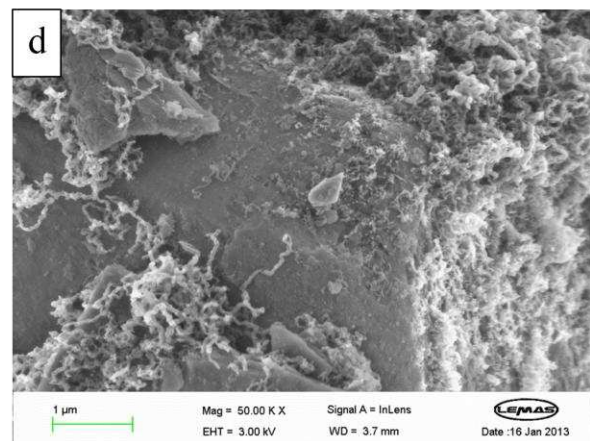
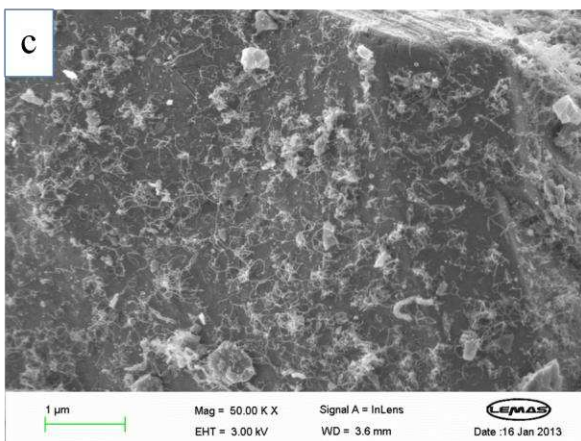
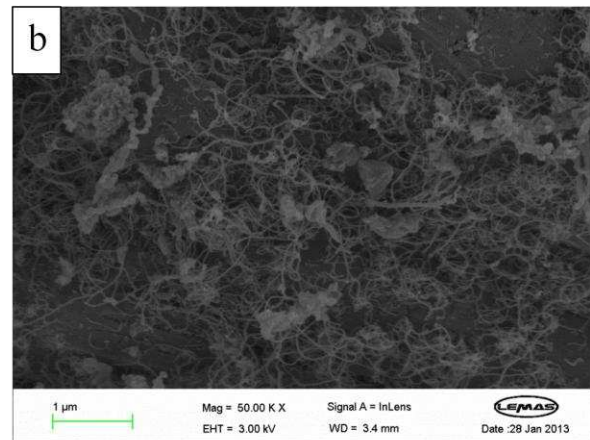
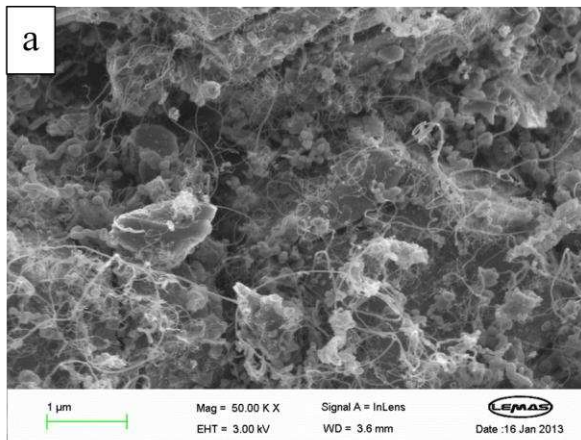


Figure 8

PP (a-b) 0 steam, (c-d) 0.25 g h⁻¹ steam, (e-f) 1.90 g h⁻¹ steam and (g-h) 4.74 g h⁻¹ steam

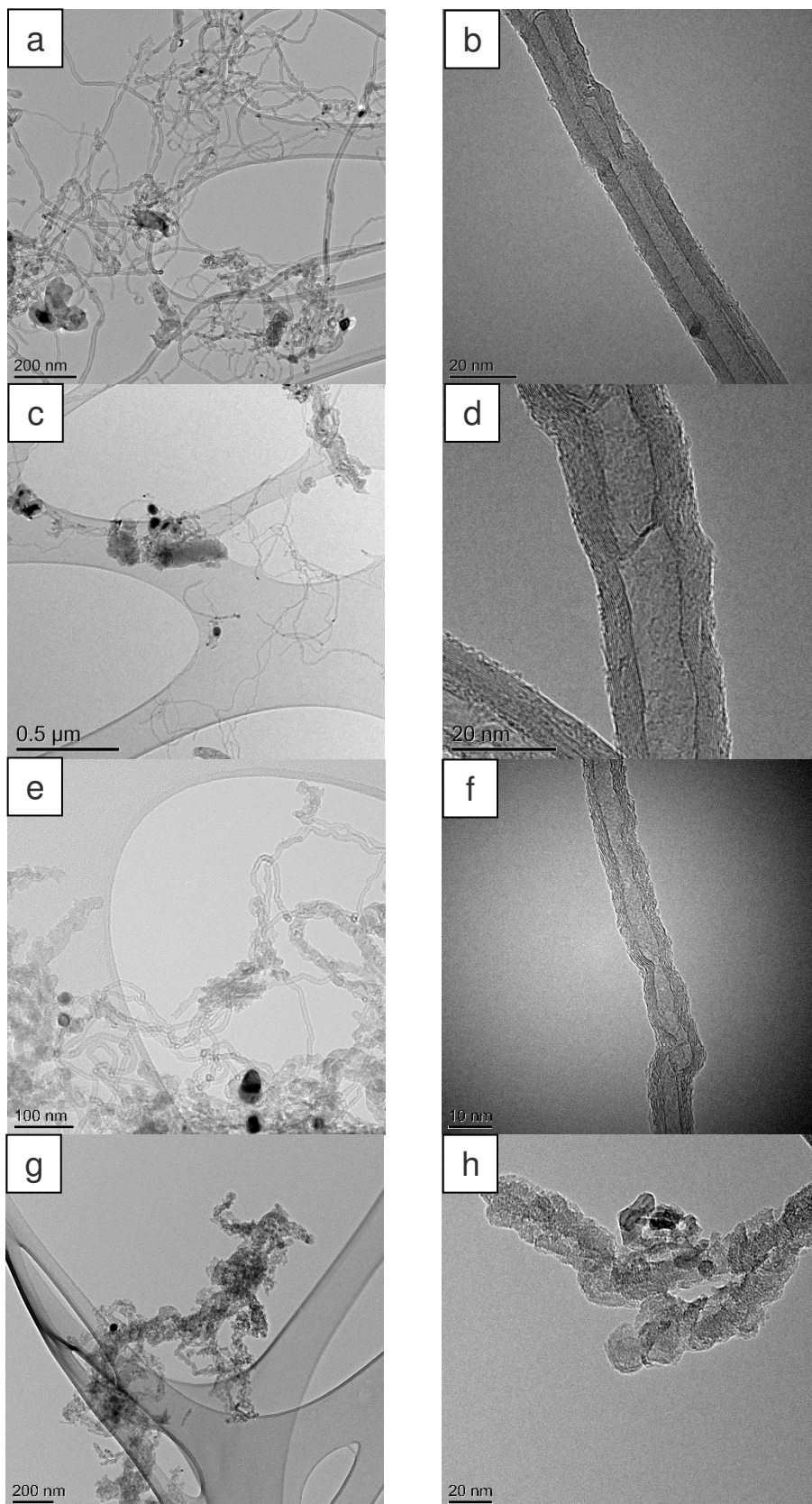


Figure 9

Raman spectrums for carbon deposits from PP with (a) 0 steam injection, (b) 0.25 g h^{-1} steam injection, (c) 1.90 g h^{-1} steam injection and (d) 4.74 g h^{-1} steam injection

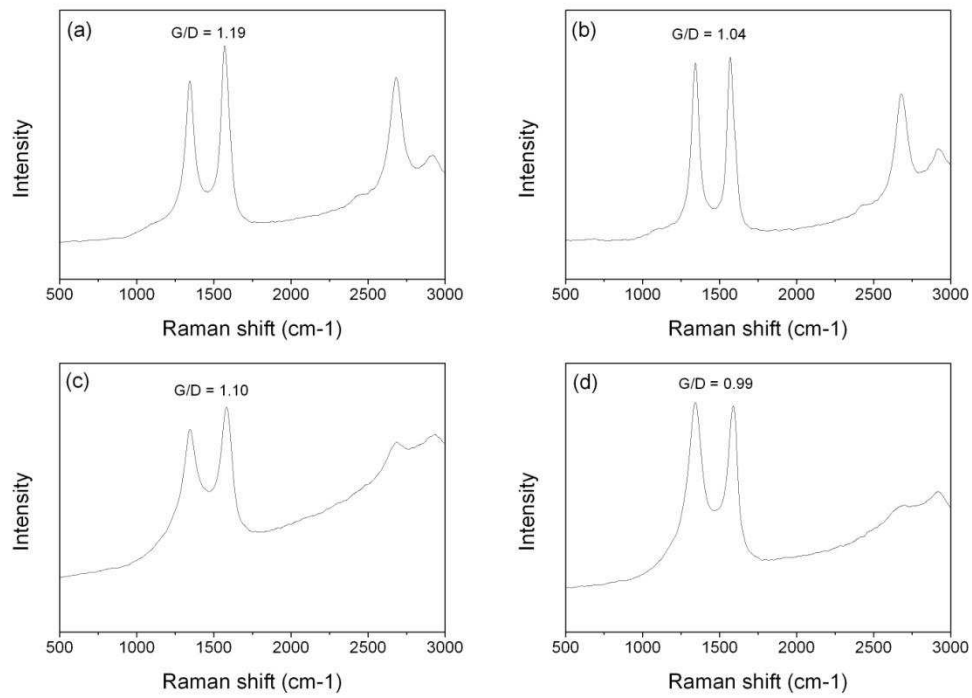


Figure 10

SEM images of carbon deposits obtained from PS at steam flow rates of (a) 0 g h^{-1} , (b) 0.25 g h^{-1} , (c) 1.90 g h^{-1} and (d) 4.74 g h^{-1}

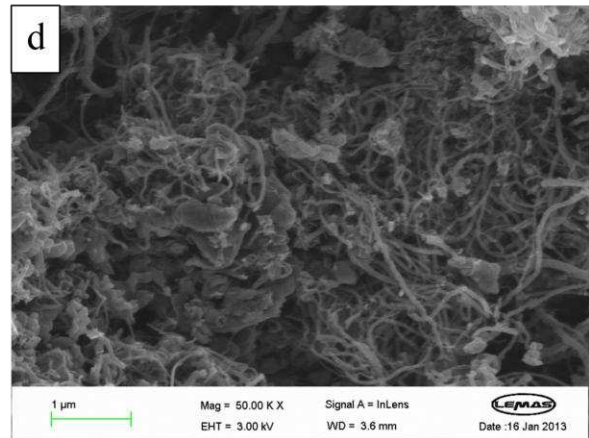
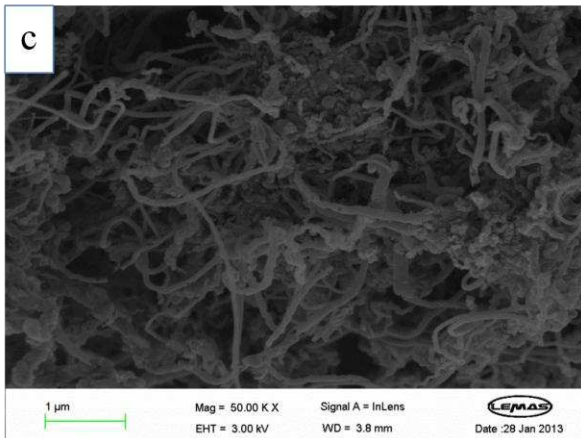
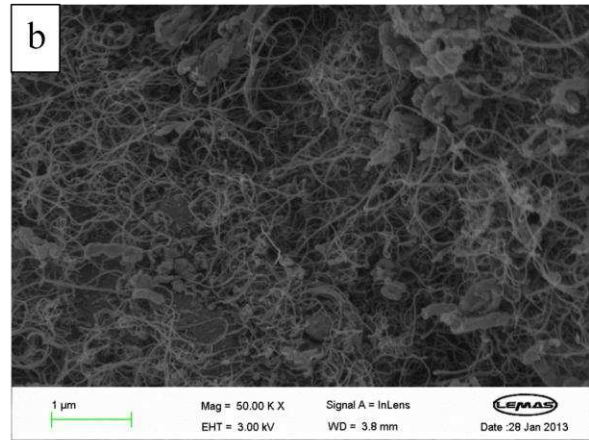
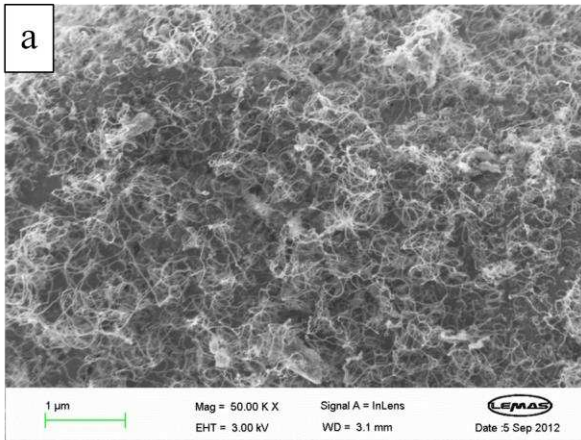


Figure 11

PS (a-b) 0 steam, (c-d) 0.25 g h⁻¹ steam, (e-f) 1.90 g h⁻¹ steam and (g-h) 4.74 g h⁻¹ steam

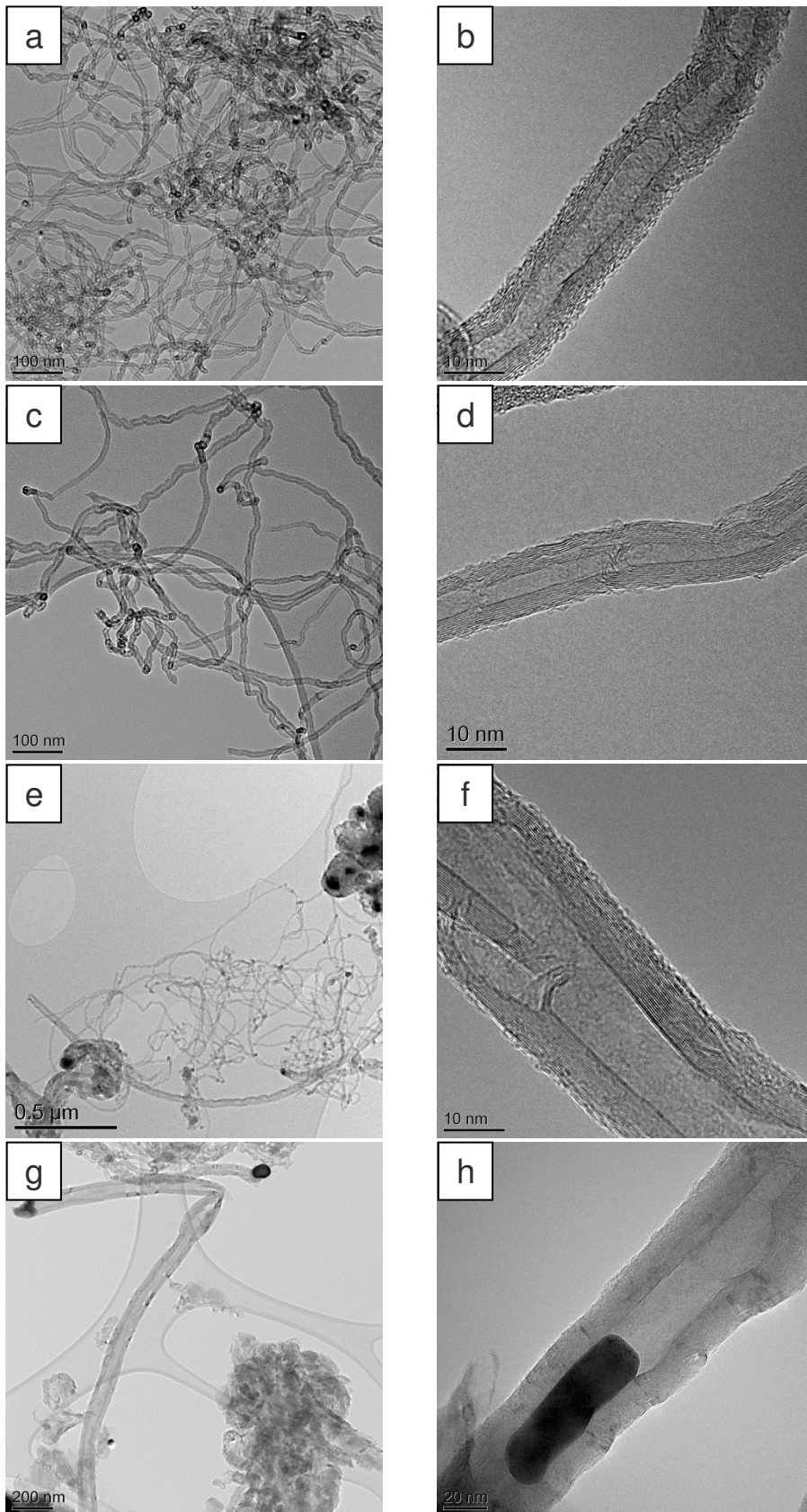


Figure 12

Raman spectrums for carbon deposits from PS with (a) 0 steam injection, (b) 0.25 g h^{-1} steam injection, (c) 1.90 g h^{-1} steam injection and (d) 4.74 g h^{-1} steam injection

